Effects of the atomic order on the half-metallic electronic structure in the $Co_2Fe(Ga_{0.5}Ge_{0.5})$ Heusler alloy thin film

K. Goto,[1,2] L. S. R. Kumara,[3] Y. Sakuraba,[1,*] Y. Miura,[1] I. Kurniawan,[1,2] A. Yasui,[3] H. Tajiri,[3] Y. Fujita,[1,4] Z. Chen,[1,2] and K. Hono[1,2]

[1]*Research Center for Magnetic and Spintronic Materials, National Institute for Materials Science, 1-2-1 Sengen, Tsukuba 305–0047, Japan*
[2]*Graduate School of Pure and Applied Sciences, University of Tsukuba, Sengen, Tsukuba 305–0047, Japan*
[3]*Center for Synchrotron Radiation Research, Japan Synchrotron Radiation Research Institute, Hyogo 679–5198, Japan*
[4]*International Center for Young Scientists, National Institute for Materials Science, Tsukuba 305–0047, Japan*

(Received 31 July 2020; accepted 15 October 2020; published 9 November 2020)

The atomic order and its effect on the electronic structure is a key issue in the application of half-metallic Heusler alloys as spin-polarized electron sources. In this study, we investigated the atomic ordering and electronic structures of $Co_2Fe(Ge_{0.5}Ga_{0.5})$ (CFGG) Heusler alloy thin films at various annealing temperatures using anomalous x-ray diffraction (AXRD) and hard x-ray photoelectron spectroscopy (HAXPES). AXRD measurements clearly showed that the Co-Fe disorder is large in the as-deposited state, which is reduced to almost zero by annealing at $T_{an} = 500\,^{\circ}C$ for 30 min. The reduction of the Co-Fe disorder explains the observed increase in the spin polarization of currents estimated by ordinary and anisotropic magnetoresistance measurements. The photoelectron spectra of the valence band in CFGG thin films with different T_{an} agree well with the first-principles calculations that considers the atomic disorder. We also found that the characteristic peaks appearing in the valence band HAXPES spectra shifted to higher binding energies, compared to the calculated density of states for stoichiometric $L2_1$-ordered CFGG. This indicates that the Fermi level is shifted and located in the vicinity of the conduction band edge in the present CFGG thin film due to electron doping by a mildly Co-rich chemical composition. Our first-principles calculations of partial density of state of *sp* electron predicted that the high spin-polarization is obtainable in a wider energy region near Fermi level in the $L2_1$-ordered structure than the B2 structure, which explains the enhancement of spin-polarization by promoting $L2_1$-ordering in the present CFGG film.

DOI: 10.1103/PhysRevMaterials.4.114406

I. INTRODUCTION

Half-metals are one of the most promising materials for spintronics applications because they exhibit high spin polarizations (P) of the conduction electrons. This is due to the absence of density of states (DOS) in only one (up or down) spin channel at the Fermi level (E_F). Co-based full-Heusler alloys, such as Co_2MnSi (CMS) and $Co_2Fe(Ga_{0.5}Ge_{0.5})$ (CFGG), are promising half-metallic materials for practical applications because of their high Curie temperatures [1,2]. Significantly high magnetoresistance (MR) effects have been widely observed in various spintronic devices, such as magnetic tunnel junctions (MTJs) [3–5], current-perpendicular-to-plane giant magnetoresistive (CPP-GMR) [6–11], and nonlocal spin-valve devices [12,13], using various Co-based full-Heusler alloys, indicating a high P. High spin-polarization over 90% was experimentally detected using spin-resolved photoemission spectroscopy [14,15]. However, fundamental understanding of the relationship between the atomic order and the electronic structure (i.e., the influence of atomic order on the spin polarization) is still lacking. To realize high P for Co-based full-Heusler alloys at room temperature (RT) for practical applications, the correlation between the degree of order and the spin polarization of Co-based Heuser alloys must be established experimentally.

The Full-Heusler alloy has an atomic formula given by X_2YZ, with an $L2_1$-ordered structure and a space group $Fm\bar{3}m$. However, in the full-Heusler film grown by the sputtering process, there are partial disorders such as the Y-Z disordering $X_2(Y, Z)$ and X-Y disordering $(X_2, Y)Z$, which are called the B2 and $D0_3$ structures, respectively. In the Co-based full-Heusler alloys, Co atoms are located at X sites, and hence they are described as Co_2YZ. It was theoretically predicted that the half-metallic electronic structure in Heusler alloys is sensitive to these atomic disorders or antisite lattice defects. Picozzi *et al.* theoretically studied the effect of atomic disorders on the electronic band structure of CMS by *ab initio* calculations, and found that the Co_{Mn} antisite (Co atom occupying the Mn site) can destroy the half-metallic gap due to the formation of an in-gap state [16]. Moreover, they also predicted that the B2 disorder (disorder between Mn and Si) does not degrade the half-metallic electronic structure. Theoretically, the B2 structure is sufficient to obtain the half-metallic electronic structure, which is commonly applicable to Co_2YZ Heuser alloys. This is because the half-metallic gap forms by the electronic bands originating from Co in Co_2YZ [2,17,18]. However, Li *et al.* reported the enhancement of the

*Corresponding author: SAKURABA.Yuya@nims.go.jp

MR ratio in the CPP-GMR device with a CFGG/Ag/CFGG structure by improving the degree of the $L2_1$-order from the B2 structure, upon increasing the annealing temperature from 500 to 600 °C in the experiment [9]. Sakuraba *et al.* also found an increase in the MR ratio in CMS/Ag/CMS, while promoting $L2_1$-ordering [7]. Therefore, there is a clear disagreement between previous theoretical predictions and experimental results in terms of the relationship between the atomic order and spin polarization.

To understand the discrepancy between theoretical predictions and experimental results, the effects of the atomic ordering on the electronic structure should be investigated. Therefore, it is necessary to clarify how the Co antisite or disorder between Co and Fe/Mn ($D0_3$ disorder) affects the half-metallic electronic structure experimentally. Standard x-ray diffraction (XRD) using a laboratory x-ray source, such as CuK_α, cannot distinguish the differences in the atomic locations of Co, Mn, and Fe owing to their close atomic scattering factors, and no quantitative analysis of Co antisite and $D0_3$ disorder for various annealing temperatures has been performed. Using nuclear magnetic resonance spectroscopy, Rodan *et al.* investigated the amount of Co_{Mn} antisite in the CMS thin films annealed at different temperatures. However, they did not correlate the result with the spin polarization of the film [19]. Raphael *et al.* investigated antisite disorder in Co_2MnSi arc-melted bulk sample using neutron diffraction technique and found a 10–14% Co-Mn $D0_3$ disorder [20]. However, neutron diffraction technique is not suitable to measure a Heusler thin film with a nanometer range thickness used for the electrode of MTJs and GMR devices. In addition, no prior work has investigated how the electronic structure of the Heusler alloy changes with atomic ordering and/or disordering. Although hard x-ray photoelectron spectroscopy (HAXPES) is a powerful tool to directly observe the electronic band structure in the bulk region, thus far, it has been used to measure samples with highly ordered atomic structures [21,22].

In this study, we investigated the effect of the atomic ordering on the electronic structure in the CFGG thin films that yielded the highest MR ratio in previous studies on the CPP-GMR [9,10]. We grew a CFGG epitaxial thin film at RT and performed post-annealing, and thier atomic order is strictly evaluated using the AXRD method through synchrotron x-rays to extract the degree of Co-Fe disorders. Furthermore, we carried out HAXPES measurements to clarify the changes of the valence band structure in the bulk region of CFGG thin films with the degree of atomic order. Based on experimental results and theoretical calculations of the DOS, we discuss the correlation between the atomic order and the electronic structure and clarify the origin of the enhancement of P by promoting $L2_1$ ordering.

II. EXPERIMENTAL AND CALCULATION METHODS

CFGG thin films with the thickness of 50 nm were deposited on a MgO (001) single crystal substrate at ambient temperature by an ultrahigh vacuum (UHV) magnetron sputtering system (base pressure $< 3 \times 10^{-7}$ Pa) to obtain a (001)-oriented epitaxial film. First, the surface of MgO substrate was cleaned by flushing process at 600 °C and then the CFGG film was deposited from $Co_{1.95}Fe_{0.89}Ga_{0.48}Ge_{0.68}$ alloy target at RT. Then, the CFGG film was annealed at annealing temperature T_{an} for 30 min without breaking vacuum in the UHV chamber. We changed the heating rates to reach T_{an} to avoid an overshooting of the temperature; ∼14 °C/min from RT to T_1 ($= 0.8T_{ann}$), ∼3 °C/min from T_1 to T_2 ($= 0.95T_{an}$) and then ∼1 °C/min from T_2 to T_{an}. After naturally cooling down to RT, the film was capped with MgO (1 nm)/Al (1.5 nm) to prevent surface oxidation. The chemical composition of the CFGG thin film was determined as $Co_{2.06}Fe_{0.99}Ga_{0.46}Ge_{0.49}$, using x-ray fluorescence analysis with standard samples whose compositions were premeasured by inductively coupled plasma mass spectrometry. This composition of the CFGG thin film can be regarded as nearly stoichiometric, but slightly Co-rich and Ga-poor with respect to the stoichiometry of $Co_2Fe(Ge_{0.5}Ga_{0.5})$. We prepared a total of five CFGG films; as-deposited and four CFGG films annealed at different T_{an} of 300, 400, 500, and 600 °C. The crystal structure and atomic order in the CFGG thin film were characterized using laboratory-based XRD method with CuK_α radiation at room temperature. The intensities of the 111 and 002 superlattice peaks, reflecting the $L2_1$ and B2 order in stoichiometric $L2_1$-CFGG, respectively, are expressed as follows

$$I_{111} \propto |f_{Fe} - (0.5f_{Ga} + 0.5f_{Ge})|^2, \quad (1)$$

$$I_{002} \propto |2f_{Co} - (f_{Fe} + 0.5f_{Ga} + 0.5f_{Ge})|^2, \quad (2)$$

where f_{Co}, f_{Fe}, f_{Ga}, and f_{Ge} are the atomic scattering factors for Co, Fe, Ga, and Ge sites, respectively. However, the site disorder between Co and Fe cannot be detected by laboratory-based XRD as $f_{Co} \approx f_{Fe}$ for the CuK_α x-ray. Therefore, to evaluate the degree of Co-Fe ordering, AXRD measurements were carried out using synchrotron x-rays with varying energies around the Co K-absorption edge (7.709 keV) at BL13XU in SPring-8 [24,25]. The enlargement of real and imaginary parts of the anomalous dispersion term in f_{Co} enlarge at the x-ray energy of the Co K-absorption edge results in $f_{Co} \neq f_{Fe}$, and thereby the Co-Fe disorder level can be evaluated by measuring I_{111} or I_{002} [23,26–28]. As the 111 superlattice peak does not appear if a CFGG thin film has no $L2_1$-order (atomic order between Fe and Ga/Ge), measuring the 111 peak is ineffective for investigating the T_{an} dependence of Co-Fe ordering by AXRD from the as-deposited state. Instead, we measured the x-ray energy dependence of I_{002} because we observed a clear 002 peak even in the as-deposited film. The intensity of the 002 peak with the Co-Fe disorder level x is expressed by the following equation:

$$I_{002} \propto \left| 2\left(1 - \frac{x}{2}\right) f_{Co} + x f_{Fe} - (x f_{Co} + (1-x) f_{Fe} + 0.5 f_{Ga} + 0.5 f_{Ge}) \right|^2. \quad (3)$$

We simulated I_{002} and the fundamental 004 peak intensity I_{004} for various values of x and then compared the simulated I_{002}/I_{004} with the experimental results to evaluate x in the CFGG film. Note that, to evaluate x strictly, we considered a slight off-stoichiometry into the simulation and

TABLE I. The models numbered as *I*, *II*, *II, IV*, and *V* indicate the site occupation of each Co, Fe, Ga and Ge for $L2_1$, B2, B2 with Co-Fe disorder, $D0_3$ and A2 structures in stoichiometric $Co_2FeGa_{0.5}Ge_{0.5}$, respectively. The model *VI* is the site occupation in ideal $L2_1$-ordered case of the present CFGG film having an off-stoichiometry. Note that here we considered the composition of $Co_{2.05}Fe_{1.00}Ga_{0.46}Ge_{0.49}$ instead of observed composition of the film $Co_{2.06}Fe_{0.99}Ga_{0.46}Ge_{0.49}$ to simplify the structure model slightly. The model *VII* is the site occupancy with considering Co-Ga disorder that we obtained by laboratory XRD. The model *VIII* is the structure with Co-Fe disordered level x that we considered to simulate x dependence of I_{002}/I_{004} shown in Fig. 3(a).

			X -site (0,0,0) + (1/2,1/2,1/2)				Y -site (1/4,1/4,1/4)				Z -site (3/4,3/4,3/4)			
Model No.		Structure	Co	Fe	Ga	Ge	Co	Fe	Ga	Ge	Co	Fe	Ga	Ge
I	($L2_1$)	$Co_2Fe(Ga_{0.5}Ge_{0.5})$	2	0	0	0	0	1	0	0	0	0	1/2	1/2
II	(B2)	$Co_2Fe(Ga_{0.5}Ge_{0.5})$	2	0	0	0	0	1/2	1/4	1/4	0	1/2	1/4	1/4
III	(B2 with Co-Fe disorder)	$(Co_{1.33}Fe_{0.67})(Co_{0.67}Fe_{0.33}Ga_{0.5}Ge_{0.5})$	4/3	2/3	0	0	1/3	1/6	1/4	1/4	1/3	1/6	1/4	1/4
IV	($D0_3$)	$(Co_2Fe)(Ga_{0.5}Ge_{0.5})$	4/3	2/3	0	0	2/3	1/3	0	0	0	0	1/2	1/2
V	(A2)	$(Co_2FeGa_{0.5}Ge_{0.5})$	1	1/2	1/4	1/4	1/2	1/4	1/8	1/8	1/2	1/4	1/8	1/8
VI	($L2_1$ *)	$Co_2Fe(Co_{0.05}Ga_{0.46}Ge_{0.49})$	2	0	0	0	0	1	0	0	0.05	0	0.46	0.49
VII	($L2_1$ * with Co-Ga disorder)	$(Co_{1.95}Ga_{0.05})Fe(Co_{0.1}Ga_{0.41}Ge_{0.49})$	1.95	0	0.05	0	0	1	0	0	0.1	0	0.41	0.49
VIII	(AXRD analysis)		$1.95(1-x/2)$	$1.95(x/2)$	0.05	0	$1.95(x/2)$	$1-1.95(x/2)$	0	0	0.1	0	0.41	0.49

multiplied a correction factor $C^* = C_{400}/C_{200}$ to the experimentally measured I_{002}/I_{004}, where C represents a correction factor, including the Lorentz factor, polarization factor, self-absorption, and footprint corrections for each diffraction. The site occupations of each elements in the stochiometric CFGG with $L2_1$, B2, $D0_3$, and A2 structure and in the current CFGG film we considered for the analysis of Co-Fe disorder are summarized in Table I. The T_{an} dependence of the degree of orders S_{B2} and S_{L21} were evaluated using the following equations:

$$S_{B2}^{XS} = \sqrt{\frac{I_{002}^{obs}/I_{004}^{obs}}{I_{002}^{sim}/I_{004}^{sim}}}, \tag{4}$$

$$S_{L2_1}^{XS} = \sqrt{\frac{I_{111}^{obs}/I_{444}^{obs}}{I_{111}^{sim}/I_{444}^{sim}}}, \tag{5}$$

where $I_{hkl}^{obs(sim)}$ is the observed (simulated) hkl peak intensity, XS denotes an x-ray source of the measurements, and for CuK_α in laboratory XRD (XS = lab) or synchrotron x-ray (XS = SR). I_{hkl}^{sim} for XS = lab was calculated by VESTA. [29]

HAXPES was performed at the hard x-ray beamline (BL09XU) in SPring-8 [30]. The excitation x-ray energy was fixed at 8.0 keV, and the photoelectrons were detected by a hemispherical analyzer (Scienta Omicron R4000). The pass energy was set to 200 eV, and the total energy resolution was approximately 260 meV. Linearly polarized light in the horizontal (p) and vertical (s) directions were used to excite photoelectrons. All measurements were performed at 300 K.

To evaluate the variation of P with respect to T_{an}, we measured the anisotropic MR (AMR) and ordinary MR (OMR) effects in the CFGG thin films. Kokado *et al.* developed a theoretical model of AMR, and predicted that half-metallic materials must exhibit negative AMR ratio [31], which was experimentally proven for various Co-based Heusler films [27,32–34]. In addition, Bombor *et al.* reported that since the electron-magnon scattering process is prohibited in half-metallic materials because of the absence of one spin channel, Co_2FeSi shows a positive OMR ratio at a temperature T below Δ/k_B, instead of negative OMR in general ferromagnetic materials [35]. Here, Δ is the energy splitting from E_F to the conduction band edge of the half-metallic gap, and k_B is the Boltzmann constant. Therefore, measuring AMR and OMR can be an approach to investigate the spin polarization of electric currents qualitatively, that is adequate for only half-metallic Heusler alloys limitedly. Hence, both the AMR and OMR effects were measured by passing an electric current of 1 mA to the in-plane ⟨110⟩ direction of the CFGG thin film. The AMR was measured by rotating the direction of the 0.3 T magnetic field applied within the film plane. The OMR effect was measured at RT and 10 K, by sweeping the magnetic field from 0 to 9.0 T applied to the perpendicular direction of the film.

To understand the disordering effects on electronic structures of $Co_2Fe(Ga_{0.5}Ge_{0.5})$, we carried out first-principles calculations on the basis of the density-functional theory, using the Korringa-Kohn-Rostoker (KKR) method [36,37] implemented into the HUTSEPOT code [38]. The atomic-sphere approximation was used to determine the Kohn-Sham potential, and atomic disorders were described by the coherent potential approximation [39]. Both the core and valence electrons were treated within the scalar-relativistic approximation, and the scattering matrices in the KKR formalism are expanded by a basis of spherical harmonics with the maximum value of the orbital angular momentum $l_{max} = 3$. In the calculations, we adopted the local-spin density approximation of Perdew-Wang [40] for the exchange-correlation energy, and used a $20 \times 20 \times 20$ k-point mesh for the full Brillouin zone. The self-interaction-correction [41] was applied locally on the majority-spin Fe-t_{2g} orbital to reproduce the magnetization of CFGG in experiments [42].

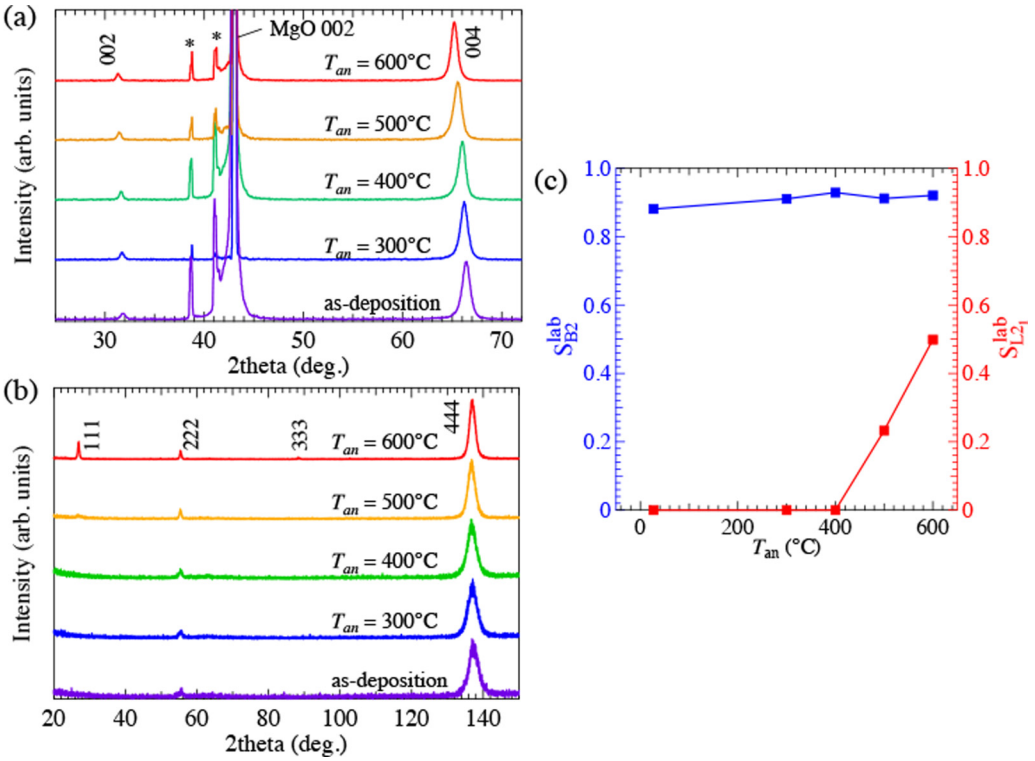

FIG. 1. θ-2θ XRD patterns for the CFGG thin film annealed at different temperature by setting the scattering vector to the (a) out-of-plane ($\chi = 0^\circ$) direction and (b) [111] ($\chi = 54.7^\circ$) direction. The peak marked with * arises from the diffractions from the MgO substrate. (c) S^{lab}_{B2} and $S^{lab}_{L2_1}$ evaluated from Eqs. (4) and (5) as a function of T_{an}.

III. RESULTS

Figure 1(a) shows the out-of-plane θ-2θ XRD pattern for the CFGG films annealed at different temperatures. Only 002 and 004 peaks were observed in the out-of-plane geometry, indicating the (001)-oriented epitaxial growth of the CFGG films. It is clearly found that the position of peaks shift toward lower angle with increasing T_{an}, indicating an enlargement of lattice constant to out-of-plane direction. This tendency can be explained by a release of in-plane tensile stress in CFGG film caused by the lattice mismatch with MgO substrate. The figure also shows a clear 002 superlattice peak in the entire range of T_{an}, even in the as-deposited state. Figure 1(b) shows the θ-2θ XRD pattern measured along the [111] direction of the CFGG film. No 111 superlattice peak is detected in the as-deposited state and the samples annealed below 400 °C, but it becomes visible in the samples annealed above 500 °C, indicating that a detectable level of $L2_1$ order appears above 500 °C. Figure 1(c) shows the T_{an} dependence of the degree of orders S^{lab}_{B2} and $S^{lab}_{L2_1}$. Interestingly, S^{lab}_{B2} is as high as ~0.9, even in the as-deposited state, and almost constant against T_{an}. This may lead to a misunderstanding that a high degree of ideal B2-order shown in the model *II* of Table I exists even in the as-deposited CFGG film. However, as indicated by Eq. (2), I_{002} does not reflect the disordering between Co and Fe because $f_{Co} \approx f_{Fe}$; thus, the estimated large S^{lab}_{B2} indicates only a high percentage of site occupancy of Ga and Ge atoms in the Y/Z site. Namely, we cannot distinguish the structure having an atomic order in between the models *II* and *III* in Table I from the result of lab XRD. We also evaluated $S^{lab}_{L2_1}$ using the extended Webster model proposed by Takamura *et al.* because S^{lab}_{B2} is smaller than 1 [43]. $S^{lab}_{L2_1}$ is zero from the as-deposited state to $T_{an} = 400^\circ$C and then increases up to 0.5 from 500 to 600 °C. Therefore, the degree of the $L2_1$-order is not perfect even at $T_{an} = 600^\circ$C in this CFGG film.

Figures 2(a) and 2(b) show the perpendicular magnetic field dependence of the electric resistivity ρ (OMR effect) in CFGG thin films measured at 10 and 300 K, respectively. The rapid variation of ρ from 0 to about 1.5 T arises from the signal from the AMR, because the magnetization direction changes from in-plane to perpendicular directions to the film plane in this magnetic field region. Thus, the OMR ratio is defined as $\Delta\rho(=\rho-\rho_0)/\rho_0$ with $\rho_0 = \rho(1.5T)$. Although the positive OMR ratio was not observed in the entire range of T_{an} even at 10 K in the present CFGG thin films, the slope of $\Delta\rho/\rho_0$ as a function of the magnetic field at 10 K clearly reduces with increasing T_{an} from the as-deposited state to 600 °C. Based on the arguments in Ref. [35], this result suggests that the suppression of electron-magnon scattering becomes stronger with T_{an}, due to the improvement of the half-metallicity. The negative OMR ratio becomes larger at 300 K than that at 10 K, but the tendency with respect to T_{an} is similar to that at 10 K, as summarized in Fig. 2(c).

Figure 2(d) shows the T_{an} dependence of the AMR ratio in CFGG thin films at 300 and 10 K. The negative AMR ratio, which has been considered as a necessary (not sufficient) condition of half-metals, was observed over the entire T_{an} range,

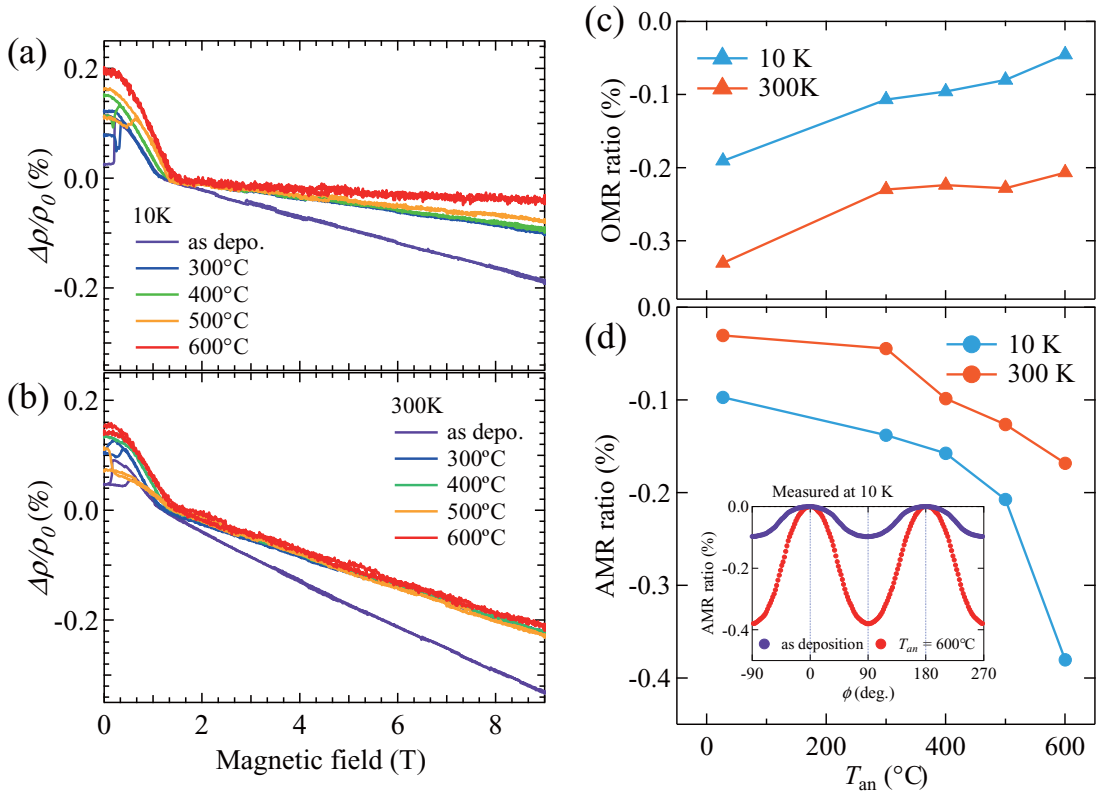

FIG. 2. Perpendicular magnetic field dependence of the OMR ratio in different annealed CFGG thin films measured at (a) 300 K and (b) 10 K. (c) T_{an} dependence of the OMR ratio in the magnetic field of 9.0 T measured at 300 and 10 K. (d) T_{an} dependence of the AMR ratio in CFGG thin films measured at 300 and 10 K. The inset shows the φ dependences of AMR ratio in the as-deposited and 600 °C annealed CFGG thin films measured at 10 K.

but its magnitude increased monotonically with T_{an}. Previous studies also found that the magnitude of negative AMR ratio has a positive correlation with the spin polarization of conduction electrons from comparative studies between the AMR and MR ratio in CPP-GMR devices [27,32,34]. Therefore, both OMR and AMR signify that the spin polarization gradually enhances with increasing T_{an}, which cannot be explained by the T_{an} dependence of S_{B2} and S_{L21} shown in Fig. 1(c), as the high B2 order guarantees a theoretically high P.

Figures 3(a) and 3(b) show the simulated and experimental results of the x-ray energy dependence of I_{002}/I_{004} in CFGG, respectively. The simulation was performed for the different Co-Fe disorder level x based on the model *VIII* in Table I, in which we considered the Co-Ga/Ge disorder elucidated by lab-XRD. Note that, because of smaller formation energy of Co-Ga disorder than that of Co-Ge disorder (see Supplemental Material [47]), here we considered only Co-Ga disordering as the analysis model. The x-ray energy used was varied from

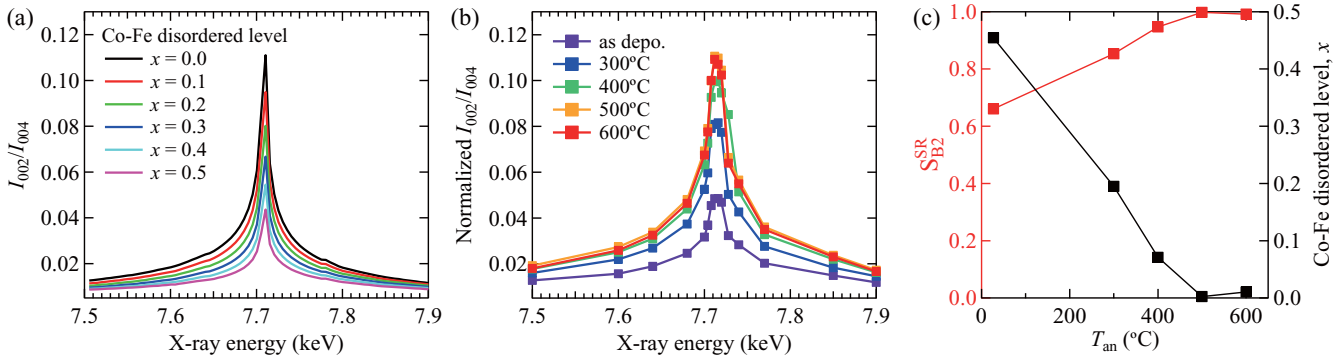

FIG. 3. (a) Simulated x-ray energy dependence of I_{002}/I_{004} in CFGG from Eq. (3) by including Co-Fe-disordered level x = 0.0–0.5. In this simulation, we considered the chemical composition and small Co and Ga disordering (shown in model *VIII* in Table I) in the CFGG thin film. (b) Experimental x-ray energy dependence of I_{002}/I_{004} in CFGG thin films annealed at different T_{an} (as-deposition and 300–600 °C). (c) S_{B2}^{SR} and the Co-Fe-disordered level x in the CFGG thin film as a function of T_{an} estimated by the comparison between the experimental and the simulated I_{002}/I_{004} intensity at the Co K-absorption edge.

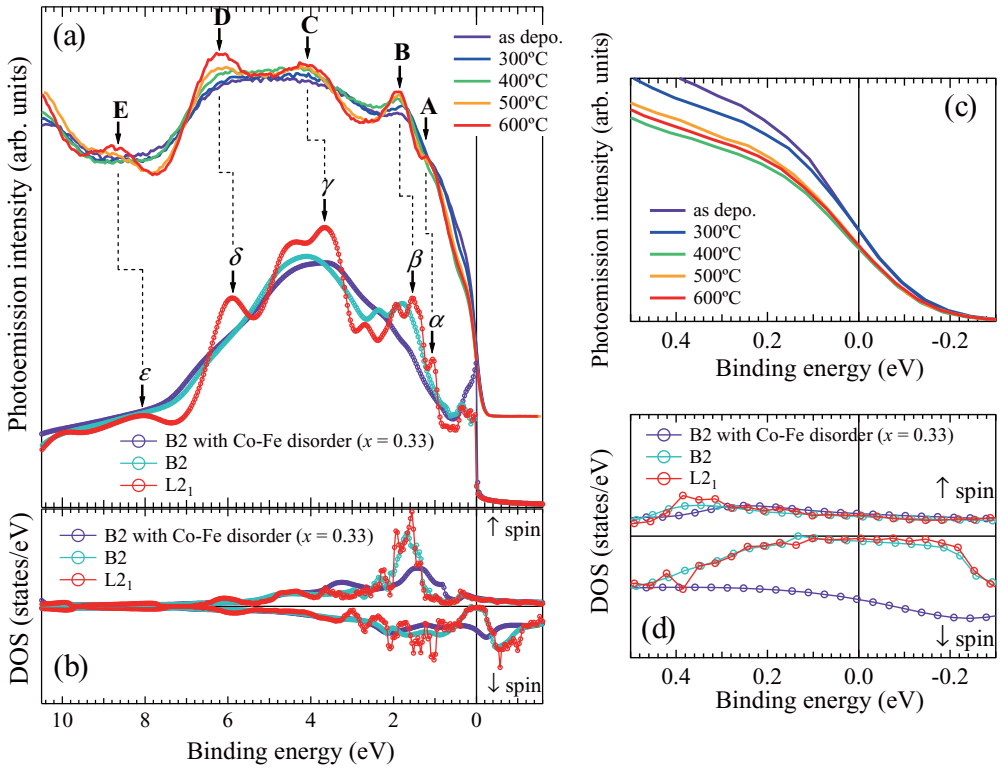

FIG. 4. (a) Valence band HAXPES spectra for the CFGG thin films with different T_{an} (upper part) and simulated photoelectron spectra for Co-Fe-disordered ($x = 0.33$) and Co-Fe-ordered ($x = 0$) B2, and $L2_1$-ordered stoichiometric CFGG using the KKR method (bottom part). (b) Calculated majority and minority spin-resolved total DOSs of Co-Fe-disordered ($x = 0.33$) and Co-Fe-ordered B2, and $L2_1$ CFGG. (c) Expanded valence band HAXPES spectra near E_F and (d) expanded calculated spin-resolved DOS near E_F.

7.5 to 7.9 keV according to the Co K-absorption edge energy. The simulation results show that the intensity ratio of I_{002}/I_{004} at the Co K-absorption edge increases with decreasing x. Interestingly, although S_{B2}^{lab} measured using a CuK_α source is nearly constant from the as-deposited state to $T_{an} = 600\,^{\circ}$C [Fig. 1(c)], we clearly detected an enhancement of I_{002}/I_{004} at the Co K-edge from the as-deposited state to $T_{an} = 500\,^{\circ}$C, indicating that the Co-Fe ordering gradually promotes with increasing T_{an} up to 500 °C. By comparing I_{002}/I_{004} at the Co K-edge between the experiment and the simulation, S_{B2}^{SR} and the degree of Co-Fe-disordered level x is estimated to be 0.66 and 0.46 in the as-deposited state, respectively. Therefore, this analysis indicates that as-deposited CFGG thin film has a nearly random Co-Fe disorder. With increasing T_{an}, S_{B2}^{SR} (x) gradually increases (decreases) to nearly 1 (0) at 500 °C, indicating that a nearly perfect Co-Fe order is formed at 500 °C. We also found that x does not change from 500 to 600 °C. Therefore, the variation of atomic ordering in the CFGG thin film with T_{an} is elucidated by the systematic XRD and AXRD analysis as follows: as-deposited CFGG thin film has an almost random Co-Fe disorder with the Ga and Ge atoms on the Y/Z sites. With increasing T_{an} up to 500 °C, Co and Fe orders to B2; thus, Co and Fe tend to occupy X and Y/Z sites respectively. From 500 °C, Fe and Ga/Ge order to the $L2_1$ structure with partial B2 disorder at 600 °C. This behavior can be well explained by the calculated activation energy for exchanging the void and each atoms [44]. Namely, the Fe atom easily migrate to the void forming in the Co site because of low potential barrier, whereas Ga and Ge atoms cannot because of the energetic instability to occupy the Co site. That is a reason for only Co-Fe atomic order promotes by low temperature annealing. Therefore, the Ga and Ge atoms need to migrate to the void in the Fe site to form $L2_1$-ordered structure, whose potential barrier is much higher than that for Fe migration to the void in the Co site. Therefore, a high T_{an} over 500 °C is required to obtain $L2_1$-ordering in the CFGG film.

The upper part of Fig. 4(a) shows the integration of valence band photoelectron spectra measured by HAXPES with p- and s-polarized light for the CFGG thin films with different T_{an}. The spectra were normalized by the intensity of Co $2p_{3/2}$ core level spectra. We can see several characteristic peaks in the spectra, denoted by A–E, and these peaks become prominent with atomic ordering by annealing. The photoelectron spectra for B2-CFGG with Co-Fe disorder ($x = 0.33$, nearly corresponding to the case of the as-deposited CFGG film) and the Co-Fe-ordered B2 and $L2_1$-ordered CFGG calculated by the KKR method are shown in the bottom part of Fig. 4(a). The photoionization cross section [45,46] for constituent elements and lifetime broadening of electrons and secondary electrons are considered in the calculation. The calculated spectrum for the B2 structure with Co-Fe disorder shows no characteristic sharp peak, which is similar to the spectra for the as-deposited sample, except for the tiny peak appearing around B. In the case of an ideal B2 structure, only one specific peak is predicted to appear around β, which also agrees with peak B, which gradually becomes prominent with increasing T_{an} to 500 °C. Thus, the enlargement of peak B is explained by the

improvement of the Co-Fe order from the as-deposited state to $T_{an} = 500\,^{\circ}$C detected by AXRD. The peaks denoted as α, γ, δ, and ε in the simulated spectrum for the $L2_1$-ordered CFGG match the peaks of A, C, D, and E observed only above $T_{an} = 500\,^{\circ}$C. Therefore, the observed valence band HAXPES spectra were well reproduced by the calculation, considering the experimentally observed atomic order.

Figure 4(c) shows the valence band HAXPES spectra just below E_F. Interestingly, the photoelectron intensity largely reduces with increasing T_{an} from 300 to 400 °C. Figure 4(b) shows the calculated spin-resolved total DOS of Co-Fe-disordered ($x = 0.33$) B2, Co-Fe-ordered B2, and $L2_1$ CFGG. The majority- and minority-spin DOSs are shown in the upper and lower panels, respectively. Noticeably, the half-metallic gap in the minority-spin channel is destroyed by the Co-Fe disorder and perfectly preserved in Co-Fe-ordered B2 and $L2_1$. Note that we use the expression of "half-metal" for ferromagnets having highly spin-polarized electronic structures around E_F. Strictly speaking, there is a tiny DOS in the half-metallic gap of CFGG even in the ordered $L2_1$ structure, leading to a spin polarization of less than 100%. As can be observed in the expanded spin-resolved DOS near E_F [Fig. 4(d)], the majority-spin DOS shows almost no change, while the minority-spin DOS at E_F decreases substantially from the Co-Fe-disordered to B2-ordered structure. Therefore, the reduction of the photoemission intensity just below E_F implies the formation of a half-metallic gap by improving the Co-Fe order. In addition, we found that all peak structures, A–E, in the HAXPES spectra slightly shifted to a higher binding energy than the peaks α-ε calculated for the $L2_1$-ordered stoichiometric CFGG. These peak shifts might be caused by the effect of electron doping due to a slight enrichment of the valence electron number (N_v) by Co-rich and Ga-poor composition in the present CFGG thin films. N_v for the stoichiometric CFGG is 29.5, but 29.8 for the CFGG film. The shift levels of each peak near E_F are estimated to be approximately 150 meV for α-A, 310 meV for β-B.

IV. DISCUSSION

Based on the experimental and *ab initio* calculation results, we discuss how the atomic order influences the valence band structure near E_F and spin polarization of the CFGG thin films with varying T_{an}. Previous studies on the CPP-GMR with the CFGG electrodes reported that the resistance change area product (ΔRA) monotonically increases with T_{an} from 1.6 mΩ μm^2 in the as-deposited state to 11.3 mΩ μm^2 for $T_{an} = 600\,^{\circ}$C, suggesting an enhancement of the spin polarization of currents [9]. The present measurements of AMR and OMR also indicate that the spin polarization of currents in CFGG thin films monotonically increases from the as-deposited state to 600 °C, which is consistent with the result in CPP-GMR. Meanwhile, general laboratory-based XRD measurements show a nearly constant degree of B2 order from the as-deposited state to $T_{an} = 600\,^{\circ}$C, and an improvement of the $L2_1$-order from $T_{an} = 500$–$600\,^{\circ}$C. Therefore, based on the theoretical prediction that the B2 order is sufficient to obtain high P in Co-based Heusler alloys, there is a clear disagreement between experimentally observed spin polarization of currents and the atomic order estimated by the general laboratory-based XRD method. Our AXRD measurements using synchrotron x-rays clarified the reason for this disagreement. A plenty of Co-Fe disorder in CFGG destroying the half-metallic gap exists in the as-deposited CFGG thin film, and gradually reduces with increasing T_{an}, and vanishes at 500 °C. As a clear half-metallic gap is expected to form with the Co-Fe-ordered B2, the monotonic increase of the spin polarization with T_{an} to 500 °C is attributable to the reduction of the Co-Fe-disordered level x. However, because x does not change above 500 °C, the improvement of the spin polarization from 500 to 600 °C is not explained by the presence of the Co-Fe disorder. As only the degree of the $L2_1$-order ($S^{lab}_{L2_1}$) increases above 500 °C, there must be a positive effect on the spin polarization by promoting $L2_1$ ordering. As electrons belonging to the s and p bands predominantly contribute to the electric conduction because of their large Fermi velocities, we calculated the energy dependence of the spin polarization in the partial DOS of sp electronic bands (P_{sp}) in B2- and $L2_1$-ordered CFGG, as shown in Fig. 5(a). As shown in Fig. 4(b), a clear half-metallic gap appears in calculated spin-resolved DOS for both B2 and $L2_1$ structures; thus, P_{sp} exhibits a similar energy dependence, reflecting a half-metallic gap. A very large P_{sp} of over 90% is obtained at E_F in both structures. However, we noticed that the energy range for high P_{sp} is different between $L2_1$ and B2; much wider in the $L2_1$-ordered structure (∼650 meV) than that in the B2 structure (∼300 meV), although the size of the half-metallic gap of the total DOS is almost comparable [Fig. 4(d)]. To show a change in P_{sp} from B2 to $L2_1$ more clearly, Fig. 5(b) shows the difference in P_{sp} between that in B2 and $L2_1$ (ΔP_{sp}). It was found that the energy range where we can obtain a comparable

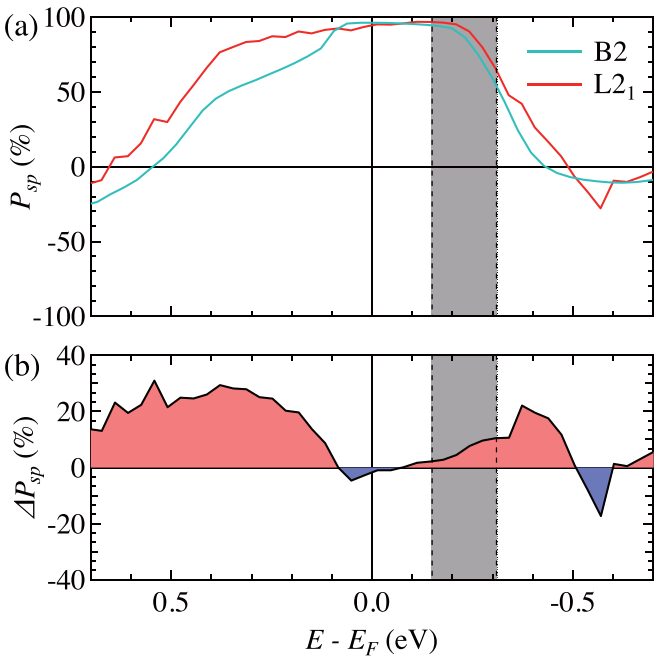

FIG. 5. Calculated energy dependence of (a) spin polarization in the partial DOS of sp conduction electrons in B2- and $L2_1$-ordered CFGG and (b) the difference of P_{sp} between that in B2 and $L2_1$ (ΔP_{sp}). The energy region highlighted in gray shows the expected position of E_F in present CFGG films from the HAXPES spectra.

P_{sp} between B2 and $L2_1$ is very narrow ($|E-E_F| \lesssim 0.1$ eV). In the energy range exceeding this narrow region around the E_F, $L2_1$ structure is predicted to have a higher P_{sp} by approximately 10 to 30% than B2 structure. Therefore, this calculation indicates that the $L2_1$ ordered structure is preferable to obtain a stability of high P with respect to the change in the position of E_F and thermal fluctuation at finite temperature. As mentioned above, based on the HAXPES spectra [Figs. 4(a) and 4(c)], the E_F in the present CFGG films shifts towards higher energy by 150–310 meV due to electron doping caused by Co-rich, Ga-poor composition. As the calculation of P_{sp} in Fig. 5 was performed for ideal stoichiometric CFGG, this electron doping is expected to push the position of E_F up to the vicinity of the conduction band edge of the half-metallic gap in the present CFGG thin films [the highlighted region in Figs. 5(a) and 5(b)]. The absence of a positive OMR ratio in our CFGG thin films (shown in Fig. 2) also supports very small energy splitting Δ or overlapping of E_F with the conduction band edge. Thus, it is inferred that the enlargement of P from B2 to $L2_1$ is more remarkable in the present CFGG thin film, because the enlargement of P from B2 to $L2_1$ becomes larger when the position of E_F is closer to that of the half-metallic gap edges. To corroborate this argument, we prepared another epitaxial CFGG film having nearly stochiometric but slightly Co-poor, Ga-rich composition ($N_V = 29.2$) for comparison. A positive OMR ratio was clearly observed at low temperatures in this CFGG film annealed at 600 °C [47], suggesting that the E_F is located below the E_F of the present Co-rich Ga-poor CFGG film, as expected from the N_V. Therefore, an improvement in the spin polarization of the CFGG thin film annealed at 500 °C to that annealed at 600 °C is explained by the expansion of the band gap for the minority *sp* electrons by ordering from the B2 to the $L2_1$ structure.

V. CONCLUSION

In this study, we investigated the atomic order in $Co_2Fe(Ge_{0.5}Ga_{0.5})$ Heusler alloy thin film annealed at different temperatures by AXRD and its effect on the half-metallic electronic structure by HAXPES. We prepared a series of CFGG films annealed at different temperature T_{an} (from 300 to 600 °C) for 30 min. Although the standard XRD using a Cu-K_α source detected a clear 002 superlattice peak for the B2-order in the as-deposited CFGG, AXRD indicated the presence of substantial Co-Fe disorder, which causes the low spin polarization in the as-deposited film even in the B2 structure. With increasing T_{an}, the Co-Fe disorder decreases until 500 °C, which contributes to the monotonic increase of spin polarization against T_{an}, as confirmed by AMR and OMR measurements. The valence band structures measured by HAXPES agree well with those simulated using *ab initio* calculations for CFGG with a disordered structure. The valence band HAXPES spectra just below E_F show a signature indicating the formation of a half-metallic gap by Co-Fe ordering. The positions of characteristic peaks in the valence band HAXPES spectra shift to higher energy direction, compared to the simulated ones for the $L2_1$-ordered stoichiometric CFGG, suggesting that E_F in the present CFGG thin film is located at the vicinity of the conduction band edge. Our first-principles calculation found that an energy region exhibiting high spin polarization of conductive *sp* electrons is enlarged by ordering the B2 structure to the $L2_1$ structure, although a half-metallic gap forms in both structures. Therefore, the improvement of the $L2_1$-order is the reason for the enhancement of spin polarization from $T_{an} = 500$ and 600 °C. This study explains the excellent MR properties reported for CPP-GMR devices with $L2_1$-ordered CFGG electrodes, which provides insights for further improvement of the performance of various spintronic devices using half-metallic Heusler alloys.

ACKNOWLEDGMENTS

The authors thank T. Nakatani, S. Ueda, K. Sumida, and A. Kimura, for the helpful discussions, and N. Kojima and B. Masaoka, for their technical support. This work was supported by a Grant-in-Aid for Scientific Research (S) (Grant No. 17H06152) from the Japan Society for the Promotion of Science (JSPS). The AXRD and HAXPES measurements were performed at BL13XU and BL09XU in SPring-8 (Proposal No. 2019A0926, 2019A0927, 2019A1532).

[1] S. Ishida, S. Fujii, S. Kashiwagi, and S. Asano, J. Phys. Soc. Jpn. **64**, 2152 (1995).
[2] I. Galanakis, P. H. Dederichs, and N. Papanikolaou, Phys. Rev. B **66**, 174429 (2002).
[3] Y. Sakuraba, M. Hattori, M. Oogane, Y. Ando, H. Kato, A. Sakuma, T. Miyazaki, and H. Kubota, Appl. Phys. Lett. **88**, 192508 (2006).
[4] K. Moges, Y. Honda, H.-X. Liu, T. Uemura, M. Yamamoto, Y. Miura, and M. Shirai, Phys. Rev. B **93**, 134403 (2016).
[5] T. Scheike, H. Sukegawa, T. Furubayashi, Z. Wen, K. Inomata, T. Ohkubo, K. Hono, and S. Mitani, Appl. Phys. Lett **105**, 242407 (2014).
[6] T. Iwase, Y. Sakuraba, S. Bosu, K. Saito, S. Mitani, and K. Takanashi, Appl. Phys. Express **2**, 063003 (2009).
[7] Y. Sakuraba, K. Izumi, T. Iwase, S. Bosu, K. Saito, K. Takanashi, Y. Miura, K. Futatsukawa, K. Abe, and M. Shirai, Phys. Rev. B **82**, 094444 (2010).
[8] T. M. Nakatani, T. Furubayashi, S. Kasai, H. Sukegawa, Y. K. Takahashi, S. Mitani, and K. Hono, Appl. Phys. Lett. **96**, 212501 (2010).
[9] S. Li, Y. K. Takahashi, T. Furubayashi, and K. Hono, Appl. Phys. Lett. **103**, 042405 (2013).
[10] J. W. Jung, Y. Sakuraba, T. T. Sasaki, Y. Miura, and K. Hono, Appl. Phys. Lett. **108**, 102408 (2016).
[11] J. Sato, M. Oogane, H. Naganuma, and Y. Ando, Appl. Phys. Express **4**, 113005 (2011).
[12] S. Shirotori, S. Hashimoto, M. Takagishi, Y. Kamiguchi, and H. Iwasaki, Appl. Phys. Express **8**, 023103 (2015).
[13] I. Ikhtiar, S. Kasai, A. Itoh, Y. K. Takahashi, T. Ohkubo, S. Mitani, and K. Hono, J. Appl. Phys. **115**, 173912 (2014).
[14] M. Jourdan, J. Minár, J. Braun, A. Kronenberg, S. Chadov, B. Balke, A. Gloskovskii, M. Kolbe, H. J. Elmers, G. Schönhense, H. Ebert, C. Felser, and M. Kläui, Nat. Commun. **5**, 3974 (2014).

[15] S. Andrieu, A. Neggache, T. Hauet, T. Devolder, A. Hallal, M. Chshiev, A. M. Bataille, P. Le Fèvre, and F. Bertran, Phys. Rev. B **93**, 094417 (2016).
[16] S. Picozzi, A. Continenza, and A. J. Freeman, Phys. Rev. B **69**, 094423 (2004).
[17] Y. Miura, M. Shirai, and K. Nagao, J. Appl. Phys. **95**, 7225 (2004).
[18] I. Galanakis, K. Özdoğan, B. Aktaş, and E. Şaşioğlu, Appl. Phys. Lett. **89**, 042502 (2006).
[19] S. Rodan, A. Alfonsov, M. Belesi, F. Ferraro, J. T. Kohlhepp, H. J. M. Swagten, B. Koopmans, Y. Sakuraba, S. Bosu, K. Takanashi, B. Büchner, and S. Wurmehl, Appl. Phys. Lett. **102**, 242404 (2013).
[20] M. P. Raphael, B. Ravel, Q. Huang, M. A. Willard, S. F. Cheng, B. N. Das, R. M. Stroud, K. M. Bussmann, J. H. Claassen, and V. G. Harris, Phys. Rev. B **66**, 104429 (2002).
[21] S. Ouardi, G. H. Fecher, and C. Felser, J. Electron Spectros. Relat. Phenomena **190**, 249 (2013).
[22] R. Fetzer, S. Ouardi, Y. Honda, H. Liu, S. Chadov, B. Balke, S. Ueda, M. Suzuki, T. Uemura, M. Yamamoto, M. Aeschlimann, M. Cinchetti, G. H. Fecher, and C. Felser, J. Phys. D **48**, 164002 (2015).
[23] B. Ravel, J. O. Cross, M. P. Raphael, V. G. Harris, R. Ramesh, and L. V Saraf, Appl. Phys. Lett. **81**, 2812 (2002).
[24] O. Sakata, Y. Furukawa, S. Goto, T. Mochizuki, T. Uruga, K. Takeshita, H. Ohashi, T. Ohata, T. Matsushita, S. Takahashi, H. Tajiri, T. Ishikawa, M. Nakamura, M. Ito, K. Sumitani, T. Takahashi, T. Shimura, A. Saito, and M. Takahasi, Surf. Rev. Lett. **10**, 543 (2003).
[25] H. Tajiri, H. Yamazaki, H. Ohashi, S. Goto, O. Sakata, and T. Ishikawa, J. Synchrotron Rad. **26**, 750 (2019).
[26] S. Li, T. Nakatani, K. Masuda, Y. Sakuraba, X. D. Xu, T. T. Sasaki, H. Tajiri, Y. Miura, T. Furubayashi, and K. Hono, Acta Mater. **142**, 49 (2018).
[27] S. Li, Y. K. Takahashi, Y. Sakuraba, N. Tsuji, H. Tajiri, Y. Miura, J. Chen, T. Furubayashi, and K. Hono, Appl. Phys. Lett. **108**, 122404 (2016).
[28] S. Yamada, S. Kobayashi, A. Masago, L. S. R. Kumara, H. Tajiri, T. Fukushima, S. Abo, Y. Sakuraba, K. Hono, T. Oguchi, and K. Hamaya, Phys. Rev. B **100**, 195137 (2019).
[29] K. Momma and I. Fujio, J. Appl. Crystallogr. **44**, 1272 (2011).
[30] E. Ikenaga, A. Yasui, N. Kawamura, M. Mizumaki, S. Tsutsui, and K. Mimura, Synchrotron Radiat. News **31**, 10 (2018).
[31] S. Kokado, M. Tsunoda, K. Harigaya, and A. Sakuma, J. Phys. Soc. Jpn. **81**, 024705 (2012).
[32] Y. Sakuraba, S. Kokado, Y. Hirayama, T. Furubayashi, H. Sukegawa, S. Li, Y. K. Takahashi, and K. Hono, Appl. Phys. Lett. **104**, 172407 (2014).
[33] F. J. Yang, Y. Sakuraba, S. Kokado, Y. Kota, A. Sakuma, and K. Takanashi, Phys. Rev. B **86**, 020409R (2012).
[34] J. Chen, Y. Sakuraba, K. Masuda, Y. Miura, S. Li, S. Kasai, T. Furubayashi, and K. Hono, Appl. Phys. Lett. **110**, 242401 (2017).
[35] D. Bombor, C. G. F. Blum, O. Volkonskiy, S. Rodan, S. Wurmehl, C. Hess, and B. Büchner, Phys. Rev. Lett. **110**, 066601 (2013).
[36] J. Korringa, Physica **13**, 392 (1947).
[37] W. Kohn and N. Rostoker, Phys. Rev. **94**, 1111 (1954).
[38] M. Däne, M. Lüders, A. Ernst, D. Ködderitzsch, W. M. Temmerman, Z. Szotek, and W. Hergert, J. Phys. Condens. Matter **21**, 045604 (2009).
[39] P. Soven, Phys. Rev. **156**, 809 (1967).
[40] J. P. Perdew and Y. Wang, Phys. Rev. B **45**, 13244 (1992).
[41] M. Lüders, A. Ernst, M. Däne, Z. Szotek, A. Svane, D. Ködderitzsch, W. Hergert, B. L. Györffy, and W. M. Temmerman, Phys. Rev. B **71**, 205109 (2005).
[42] Bsdc. Varaprasad, A. Srinivasan, Y. Takahashi, M. Hayashi, A. Rajanikanth, and K. Hono, Acta Mater. **60**, 6257 (2012).
[43] Y. Takamura, R. Nakane, and S. Sugahara, J. Appl. Phys. **105**, 07B109 (2009).
[44] H. Tajiri, L. S. R. Kumara, Y. Sakuraba, T. Nakatani, J. W. Jung, and K. Hono (unpublished).
[45] M. B. Trzhaskovskaya, V. I. Nefedov, and V. G. Yarzhemsky, At. Data Nucl. Data Tables **77**, 97 (2001).
[46] M. B. Trzhaskovskaya, V. I. Nefedov, and V. G. Yarzhemsky, At. Data Nucl. Data Tables **82**, 257 (2002).
[47] See Supplemental Material at http://link.aps.org/supplemental/10.1103/PhysRevMaterials.4.114406 for details on ordinary magnetoresistance effect in another CFGG film having smaller valence electron number.